A Fabry–Pérot Cavity for Rare-Earth-Ion-Doped Nanocrystals

Thesis for the degree of Bachelor of Science,
Project Duration: 3 months

André Nüßlein

LUNDS UNIVERSITET

Supervisor: Andreas Walther
Semester: Autumn 2018
Department of Physics
Division: Atomic Physics

Abstract

This thesis work contributes to the effort of detecting single rare earth ions doped into crystals, an operation crucial for the development of rare earth quantum computer hardware. Doping crystals with rare earth elements, their trivalent ions substitute some of the crystal's original bonds. These ions have a partially filled 4f shell, protected by the full 5s and 5p shell from the environment which makes them good candidates for qubits.

Because not every ion experiences the same electric field from the imperfect crystal, their total linewidth is inhomogeneously broadened. If the doping is sufficiently low and the crystal sufficiently small, each ion undergoes a different optical shift and can thus be addressed separately. Communication between ions happens due to their permanent dipole moments which change according to their energy level.

So far no single ions could be detected in Lund because highly doped bulk crystals were used. It was nevertheless tried to construct quantum logic gates using qubits that consisted of an ensemble of ions. Constructing logic gates with these means that every single ion of one qubit needs to be able to communicate with every single ion of another qubit, a method that becomes increasingly difficult when more and more qubits are to be entangled. Connecting as many qubits as possible is a crucial step in building a quantum computer that could outperform classical computers and this could be facilitated if every qubit consisted of only one ion which is the reason for the recent explorations towards nano crystals. This development also makes it possible to address another problem of rare earth ions, their low probability of spontaneous emission.

Placing nano crystals into an optical cavity promises the enhancement of spontaneous emission by the Purcell effect. Ideal cavities are Fiber Fabry-Pérot resonators of which one side consists of a mirror coated fiber tip and the other of a plane mirror functioning as the substrate for the nano crystals. It was the aim of this thesis to build a cryostat holder that would bring these two mirrors together with high stability and would allow for vertical and horizontal scanning.

Acknowledgements

First of all, I would like to express my gratitude towards my supervisor Andreas Walther who trusted me with a project that is not just a student project but has actual impact on the group's work. Whenever I asked him if he had time for some discussions, he made time for me. After a short hand notice of mine, he and Lars Rippe invited me to a skype talk to propose different projects. The project I chose was not necessarily connected with Lars' own work but he still kept contributing to it. Some of the most important ideas for locking and structural stability came out of his brain.

I would also like to thank Stefan Kröll for leading the Quantum Information group in such a relaxed way. Thank you also to all the wonderful colleagues in the group; Sebastian for giving me advice on what products to buy and providing me with the infamous purchase offer, Vassily for helping me find this research group, Mohammed for giving me advice on my progress and all the rest for the interesting conversations over Monday lunches and BMC food the rest of the week.

Abbreviations

CAD	computer-aided design
FEA	finite element analysis
FSR	free spectral range
FWHM	full width at half maximum
PSD	power spectral density
QED	quantum electrodynamics
REI	rare earth ions
SE	spontaneous emission

Ce	cerium
Gd	gadolinium
Eu^{3+}:Y_2O_3	europium-doped yttria
YAG	yttrium aluminium garnet
Yb	ytterbium
YSO	yttrium orthosilicate
Nd	neodymium
Pr	praseodymium

Contents

1. Introduction

In Lund, many years have gone into the research on Quantum Computing using rear earth ions (REI). One essential step that is yet to be achieved is addressing single ions. This is important for scaling quantum computers, that is, to connect as many qubits as possible together. One promising way of doing so is by placing the REI into a very small optical cavity (in the order of a few wavelengths) for which a tailor made set up would have to be designed. This method will be put into context by the remainder of this introduction and the following theory part.

The classical analogy to a quantum computer's qubit is a bit. Standard computers use bits of value either 1 or 0 as their smallest unit of information because every calculation can in principle be broken down to manipulating strings of these two numbers by logic gates (also simply called 'gates'). Quantum Computers function similarly, but to explain the extraordinary power of qubits, some elementary Quantum Mechanics has to be accepted. Teaching us that microscopic objects can be in a superposition of states, it is for example possible to have an electron simultaneously in two different levels of an atom. This electron would then carry two bits of information for the price of one. Such an arrangement can already function as a qubit, the basis for Quantum Computer Algorithms that consecutively apply quantum logic gates on these to execute calculations unsolvable with classical computers.

A text book example of such an algorithm, introduced by Peter Shor, can find the prime factors of any integer [1]. For large integers, this problem is extremely inefficient using classical computers (the computing time increasing exponentially with problem size). Quantum computers are expected to solve this problem in polynomial time (the time it takes is proportional to n^k where n is the integer to be factored and k is a positive number), an exponential improvement. This has far reaching implications because current cryptosystems rely on the fact that big numbers cannot be factorized. Luckily, there exist quantum cryptography algorithms not relying on any mathematical difficulty and these could one day be used to protect credit card transactions [2].

When these algorithms were first written, the control of qubits was still far from reality. Nowadays several methods exist to prepare qubits in desired states, communicate with them and let them communicate with each other [3]. One such method is called ion trapping in which very few ions are cooled down to very low temperatures held in place by for example an electrical field. A different way of trapping ions is pursued in Lund by incorporating them in a crystal whose structure holds the ions stable and communication can be done via laser light.

Particular types of ions are used which belong to the group of rare earths consisting of the lanthanides (with atomic numbers 57 through 71, from lanthanum through lutetium), scandium and yttrium (with atomic numbers 21 and 39). They were proposed as the hardware for quantum computers [4] and for storing quantum information [5] because of their particular

advantages such as for example their long coherence times of up to six hours [6]. Successful implementations include the preparation of individual praseodymium ions in yttrium orthosilicate (Y_2SiO_5, also called YSO) to desired electronic states [7] or the detection of the same trivalent praseodymium hosted by a yttrium aluminium garnet (YAG) crystal [8]. Because of the long fluorescent lifetimes of the $4f \leftrightarrow 4f$ transitions (more about this in the theory subsection 2.1.3), the ions' emission rate is very low, and in order to detect single ions, advanced laser spectroscopic techniques are needed. For the experiment in Ref. [7] crystal pieces mined from a bulk crystal were observed and for the experiment in Ref [8] nanocrystals were used. The latter were shown to be adequate hosts for rare earth ions and are apt for being coupled to nanoscale systems [9]. Their dimensions make it possible to insert them into small optical cavities, avoiding the sophisticated techniques used in [7, 8].

Trapping light between two mirrors creates what is called a cavity or a resonator. This can be done with light of different wavelengths, even with microwaves. An example of an optical cavity is the Fabry-Perot resonator which can be used to provide better communication with trapped ions. Using a high Finesse (see later sections) and a microscopic size, experiments can enter the regime of "cavity quantum electrodynamics" (cavity QED). A group that is now located in Karlsruhe has shown a way of building such a cavity where at least one of its ends is a mirror coated fiber [10, 11]. Using it, a scanning cavity microscope was built [12], the observation of Nitrogen-vacancy centres in crystals was enhanced [13, 14], it was shown that a thick diamond membrane in the cavity does not affect the cavity quality significantly [15] and carbon nanotubes were studied by Purcell enhanced Raman scattering [16].

More recently, spectroscopy of europium-doped yttria (Eu^{3+}:Y_2O_3) was cavity enhanced which is very closely related to what is planned in Lund [17]. Here, the same yttrium oxide micro crystals (Y_2O_3) will be used but they will be doped with neodymium (Nd) and praseodymium (Pr) instead. In this case, the qubit will be formed by the Pr ion, and the Nd will act only as a readout ion, an ion used to detect the qubit state but not taking part in the computation. To start working on this project, previously fabricated Fabry-Pérot resonators were attained from the group in Karlsruhe, and later on they will be custom made.

One of the cavity's mirrors can serve as a substrate for the crystals. The same mirror can be moved in the two horizontal directions so to align any crystal with the light source. The cavity length will be steered by another nano positioner moving the fiber vertically. Because this should be achieved in a second step inside a cryostat, the set up with the two mirrors and the mechanics for moving the mirrors should be confined within a cylinder of diameter less than $24\ \mathrm{mm}$, the construction of which was the main task of this Bachelor project.

Before going into the engineering details, a theoretical section will give more insights into the Quantum Computer domain and its rare earth approach. The Fabry-Perot cavity's classical properties will be explained thoroughly before quantum optical arguments will be used to motivate why such a cavity is useful to detect single ions. Because it was impossible to already confine the crystals in the cavity, the outlook will serve as a prediction of what the set up can be used for in the near future.

2. Background and Theory

2.1 Quantum computing

Every engineering effort going into this project has always been executed with having in mind that it could eventually contribute to building a quantum computer. Building on what has already been mentioned in the introduction, its foundations and possible application will be reviewed superficially but the interested reader is referred to the book by Nielsen and Chuang [18]. It will be described how rare earth ions can function as qubits, and finally it will be motivated why placing rare-earth-ion-doped crystals into optical cavities is of interest.

2.1.1 Basic principles and applications

As mentioned in the introduction, a quantum computer's basic unit is called a qubit in reference to the binary classical bit which can for example be created by exploiting the electron spin being up and/or down. This possible superposition breaks down at measurement but there exist a chance to observe either value. The hidden information before measurement scales exponentially with increasing number of entangled qubits, making computations much faster than on any imaginable classical computer. This chain of qubits needs to be as long as possible (at least around 50 [19], other computations requiring 200 million [20]) but with rare earth ions, two qubits are yet to be entangled.

Apart from Shor's algorithm, there exist other possible applications. One unique power of quantum computers is that they can simulate nature in a way that ordinary computers cannot. To explain this statement, Feynman himself breaks this down to simple terms in one of his famous speeches published in 1982 [21]. Until today he was not proven wrong as it is still inefficient to solve the equations that describe a big assembly of atoms even using modern super computers. Simulating such systems could for example prove very useful in pharmaceutical research from which society as a whole would benefit. Another, already mentioned concept is quantum cryptography. Two parties each given a state that is intrinsically connected ("entangled") to the state of the other party can exchange a decryption key via this connection. It is then possible to see whether a third party is dropping ears on the conversation, making the system bullet proof. This application is the closest to mainstream realization with several companies already offering quantum key transporting over several hundreds kilometers [22]. Quantum Computing, on the other hand, is more challenging because the algorithms require entangled states to be able to undergo change on demand. How this can be done in principle will be explained in the following.

2.1.2 Quantum logic gates

Classical logic gates are fed with one or two binary values and output one single binary. The actual value read at an input terminal is a voltage and if it is high, it will be interpreted as a 1 (and 0 otherwise). One of the most fundamental gates is called an inverter or NOT gate. It has only one input and returns exactly the opposite binary value of what it was given: it "inverts" the value. There exist seven basic gates and they are usually implemented using diodes or transistors. Most mathematical problems can be reformulated to only have the values "true" or "false" as input and these problems can then be solved using a chain of the fundamental gates.

A similar concept is used in a quantum computer with the not so surprising name "quantum logic gate", one of which, the so called "controlled-NOT" gate, will be discussed here. This gate has two input qubits, known as the "control" and the "target" qubit. After reading both qubits, the gate will only leave the target qubit unchanged if the control qubit is 0. This can be written in mathematical notation as

$$|00\rangle \to |00\rangle; \quad |01\rangle \to |01\rangle; \quad |10\rangle \to |11\rangle; \quad |11\rangle \to |10\rangle, \tag{2.1}$$

with the first number in the bracket notation representing the control qubit and its neighbour the target qubit. How such a gate is actually implemented with REI will be explained after an introduction to the ions' properties.

2.1.3 Rare-earth-ion-doped crystals

As mentioned in the introduction, it is the lanthanides, scandium and yttrium which are referred to as rare earths. Their position in the periodic table can be seen from figure 2.1.

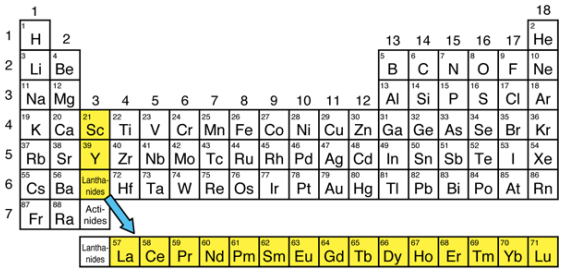

Figure 2.1: The rare earth elements in the periodic table. Figure taken from [23].

The lanthanide ions are usually found in the trivalent state RE^{3+}. The ground electronic configuration of the rare earth ions may be written as $[Kr]4d^{10}5s^25p^64f^n$ where [Kr] is the closed-shell configuration of the noble gas krypton and n is the number of electrons in the unfilled $4f^n$ shell ranging from n = 1 for Ce^{3+} to n = 13 for Yb^{3+} [24]. Because the filled $5s$ and $5p$ states are spatially extended farther out than the $4f$ electrons, they can shield the $4f$ electrons from outer disturbances (see figure 2.2). $4f - 4f$ transitions are forbidden for free ions but become weakly allowed when the ions are doped into a crystal. Being weak and well shielded, these transitions have long life and coherence times under cryogenic temperatures (≈ 4 K) resulting in very narrow and homogeneous absorption linewidths,

even when doped into crystals. Homogeneous in this context means that all ions' optical linewidths are equally increased from a delta function to a Lorentzian shaped profile.

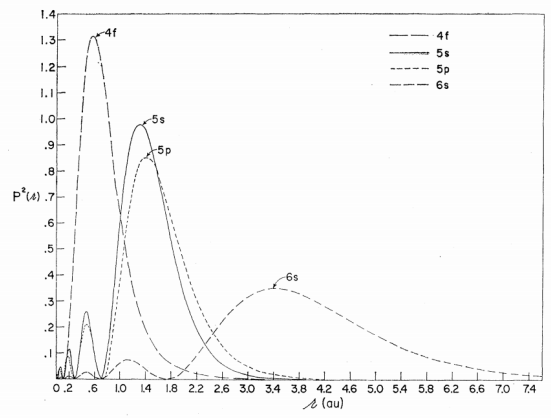

Figure 2.2: The radial distribution of $4f, 5s, 5p$ and $6s$ electron orbitals in Gadolinium (Gd) shows how the $4f$ orbital is shielded by the outer lying orbitals. Figure taken from [25].

What changes from the description of free ions to trapped ions is the electric field induced by the host crystal. The crystal is strained by the dopant ions not having the same size as the original lattice components. Because of this, and crystal imperfections, the local electric field varies from ion to ion, resulting in an absorption frequency shift and the ensemble gives rise to a broad inhomogeneous line as sketched in figure 2.3. Assuming that every ion experiences a different shift, a single ion represents a single qubit. If that is not the case, all ions that share the same frequency can be considered to make up a single qubit which is referred to as the ensemble approach as opposed to the single ion approach. One can get from the first to the second case simply by increasing the dopants' density, but the ensemble approach is much more difficult to implement because it requires all ions of one qubit to communicate with all ions of another.

When saying that a single ion is a qubit, it is meant that its two hyperfine levels in the electronic ground state correspond to the information $|0\rangle$ and $|1\rangle$, respectively. An ion could have more than two hyperfine levels but it is possible to only use two of them for operations. How then a C-Not gate can be implemented is explained thoroughly in the paper that laid the ground for Quantum Information research in Lund [4]. Its basis is that the permanent dipole moment varies between hyperfine levels. Target ions can therefore feel in which state a control ion can be found and only change state accordingly. The details for the single ion approach are provided in appendix A.

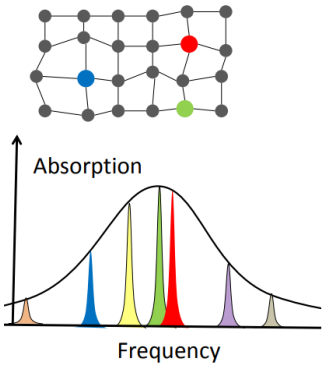

Figure 2.3: The resulting broad inhomogeneous linewidth, made up of many homogeneously broadened linewidths, each one due to random shifts of the local electric field.

As already mentioned, a qubit can in principle consist of multiple ions. For the logic gates to work, all ions making up the target qubit need to be able to feel the control qubit's dipole moment. This means that all of them have to be sufficiently close to all control ions which is statistically improbable. Similarly, connecting

more than two qubits together becomes almost impossible. It is therefore desirable to have single ions constituting one qubit, but when laser light is sent into the bulk crystal many ions will be subject to its excitation, inhibiting single ion detection. Using micro- or even nano-crystals could bypass this problem, but once the structures are so small they would be ready to be placed inside optical cavities. Why this is advantageous will be explained after detailed information of the classical properties of Fabry-Pérot cavities.

2.2 The Fabry-Pérot cavity

The light confined inside a Fabry-Pérot cavity is of the shape of a Gaussian beam. What this beam is characterized by and how one arrives at its expression, is the starting point for this section. Since it also constitutes the appropriate description for a laser beam in general, its divergence will later be used to justify the placement of a collimating lense. Why only a beam of certain frequency can survive inside a resonator is derived in the part that also introduces all relevant cavity parameters. It will then also become apparent why the cryostat holder needs to be very stable.

2.2.1 Light and the Gaussian beam

Light is an electromagnetic wave that changes sinusoidally in time [26]. Its electric field part u (and also the magnetic part) obeys the wave equation

$$\nabla^2 u - \frac{1}{c^2}\frac{\partial^2 u}{\partial t^2} = 0, \tag{2.2}$$

with c the speed of light. A function that satisfies this equation and represents a monochromatic wave is

$$u(\boldsymbol{r}, t) = a(\boldsymbol{r}) \cos\left[2\pi\nu t + \varphi(\boldsymbol{r})\right], \tag{2.3}$$

where $a(\boldsymbol{r})$ is the wave's amplitude, $\varphi(\boldsymbol{r})$ its phase and ν its frequency.

In complex notation, the wavefunction can be written as

$$U(\boldsymbol{r}, t) = U(\boldsymbol{r}) \exp(j2\pi\nu t). \tag{2.4}$$

The real representation can be obtained by adding the complex wavefunction to its complex conjugate and dividing by two. Substituting this into the wave equation gives a differential equation for the complex amplitude $U(\boldsymbol{r})$:

$$\nabla^2 U + k^2 U = 0, \tag{2.5}$$

which is known as the Helmholtz equation, where

$$k = \frac{2\pi\nu}{c} \tag{2.6}$$

is called the wavenumber.

There exist many solutions for $U(\boldsymbol{r})$ such as the simple ones that give plane or spherical waves. In the first case, the wave travels in a plane in the z direction with the wave crests forming parallel lines. The second case results from a point source where the wave crests form concentric circles around it. That a laser beam following a confined straight line cannot be adequately described by these is obvious. Instead, it is most of the time approximated to be Gaussian instead: its fundamental mode is circularly symmetric and more intense close to its axis. Even the eigenmodes of an optical cavity can be approximated this way. Here, only some results will be given which are derived in books such as "Fundamentals of Photonics" by Saleh and Teich [27]. It is also this book whose notation will be adhered to. The fundamental Gaussian beam's ($\mathrm{TEM}_{0,0}$) complex amplitude is given by

$$U(r) = A_0 \frac{W_0}{W(z)} \exp\left\{\left[-\frac{\rho^2}{W^2(z)}\right]\right\} \exp\left\{\left[-jkz - jk\frac{\rho^2}{2R(z)} + j\zeta\right]\right\}, \tag{2.7}$$

where j is the imaginary unit and $\rho = x^2+y^2$ for a beam travelling in the $z-$direction. All other parameters have the following physical interpretations that are also sketched in figure 2.4.

- The beam width $W(z) = W_0\sqrt{1+(\frac{z}{z_0})^2}$ is the radial distance at which the peak intensity ($|U(r)|^2$) has decreased by a factor $1/e^2$ from its maximum value on the beam axis. 86% of the beam's power is confined in a circle with a radius of $W(z)$. The beam diverges hyperbolically but converges to a linear function $W(z) \approx \theta_0 z$, with $\theta_0 = \lambda/(\pi W_0)$.
- The beam width's minimum value is attained at the waist radius $W_0 = \sqrt{\lambda z_0/\pi}$.
- $z_0 = \pi W_0^2/\lambda$ is called the Rayleigh range. When travelling z_0 along the beam's direction, the radius will have increased by $\sqrt{2}$.
- $R(z) = z[1+(z_0/z)^2]$ is the radius of curvature of the beam. At $z = 0$ the radius is infinite and the wavefronts are planar. $R(z)$ then quickly drops to its minimum value $2z_0$ at $z = z_0$. After this, it increases towards a linear behaviour in z and at infinity the beam resembles a spherical wave.
- $\zeta(z) = \arctan(z/z_0)$ is the Gouy phase. In comparison to a plane or a spherical wave, the Gaussian beam is delayed by this factor which ranges from $-\pi/2$ at $z = -\infty$ to $-\pi/2$ at $z = \infty$.

It is important to note that there exists another sensible set of solutions to the Helmholtz equation. Called Hermite Gaussian beams, they all share the same Gaussian wavefronts but have more complex intensity distributions. Each solution corresponds to a mode characterized by two integer numbers, l and m. Their lowest order is just the Gaussian beam described above

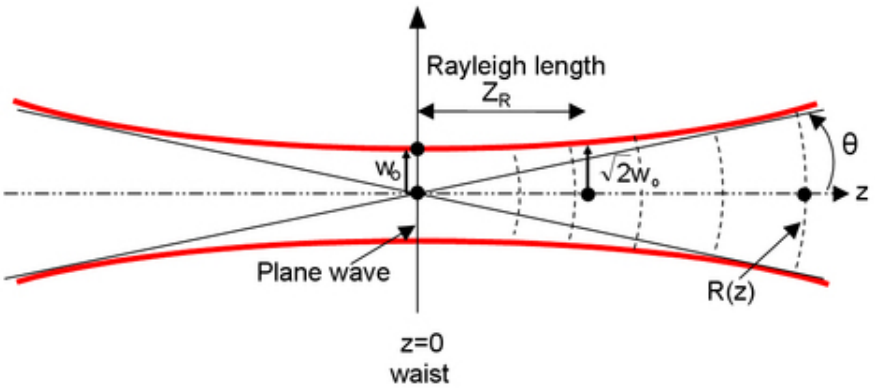

Figure 2.4: A Gaussian beam with planar wavefronts at $z = 0$ with the properties described in the main body. Figure adapted from [28].

and the others have an intensity distribution with l nodes in the horizontal direction and m in the vertical direction. Some of these might be more prone to survive in the cavity while other ones could be preferably supported by the fiber resulting in mode matching losses.

2.2.2 The resonant Fabry-Pérot cavity

Resonance frequencies

Introducing light into the space between two, partially transmitting mirrors, only certain frequencies can escape extinction from destructive interference. This is for example used to lock a laser to a specific frequency. For plane waves between plane mirrors of distance d on the z-axis, the allowed frequencies are easily derived [29]: The solution to the Helmholtz equation with the boundary conditions $U(0) = U(d) = 0$ gives $U = A\sin(kz)$ with $k = q\pi/d$ where $q = 1, 2....$ From this (and the definition of the wavenumber) we get that the round-trip distance traversed at resonance must be equal to an integer number of wavelengths:

$$\nu = q\frac{c}{2d} \quad \Rightarrow \quad q\lambda = \frac{c}{\nu} = 2d. \tag{2.8}$$

The distance between two neighbouring frequencies is therefore

$$\nu_F = \frac{c}{2d}, \tag{2.9}$$

which is referred to as the **free spectral range** (FSR). At zero transmission, the resulting frequency spectrum consists of $\delta-$functions, but for a finite transmission where light light can leak out of the resonator, these sharp peaks become Lorentzian functions around ν. While it is impossible to create perfect mirrors, it is also not desirable because then no information could be obtained. The first application of a cavity-emitter ensemble can now be understood. Scattering and absorption due to the emitters inside the cavity attenuates the light's intensity that

is coupled out of one of the mirrors. This attenuation depends on the particles' size, making microscopy possible [12]. A few more characteristics of cavities have to be introduced before their application to quantum information becomes apparent.

Finesse and quality cactor

Consider a wave reflecting back and forth between two mirrors. After each round trip, the phase is shifted by φ ($= 2kd = 4\pi\nu d/c = 2\pi\nu/c\nu_F$ which will be used later), and because of losses, the wave's amplitude is attenuated each time. The factor by which the two mirrors reduce the amplitude is called $|r|$. If the original wave has complex amplitude U_0, the reflected wave after one round trip is $U_1 = r\exp\{(-j\varphi)\}U_0$ (intensity reduced and phase shifted). This continues to give $U_2 = r\exp\{(-j\varphi)\}U_1 = r^2\exp\{(-2j\varphi)\}U_0$ and so on. But because they all coexist in the cavity, squaring their sum (calling this sum U) gives the intensity of the light in the resonator

$$I = |U|^2 = \frac{I_0}{1 + |r|^2 - 2|r|\cos\varphi}, \tag{2.10}$$

with $I_0 = |U_0|^2$, the initial intensity. This can be written as

$$I = \frac{I_{\text{max}}}{1 + (2\mathcal{F}/\pi)^2 \sin^2(\pi\nu/\nu_F)}, \quad I_{\text{max}} = \frac{I_0}{(1-|r|)^2}, \tag{2.11}$$

where the finesse $\mathcal{F}$ of the cavity is defined as

$$\mathcal{F} = \frac{\pi\sqrt{|r|}}{1-|r|}. \tag{2.12}$$

The finesse is an important value that characterizes the cavity, and its value is related to the sharpness of peaks around allowed frequencies (it should be noted that some sources like the textbooks [29] and [30] define the finesse slightly differently but its implications remain unchanged) . A high finesse is achieved with low transmissive mirrors because they have r going to unity, making $\mathcal{F}$ very large. If a laser beam of a certain frequency is introduced into a high finesse cavity, slight deviations in the cavity length d can then result in this frequency not surviving. On the other hand, one could think that the allowed frequency range should be small so to not induce other transitions, but this can be controlled by keeping the laser line small. A high finesse is still desirable because, as will be shown later, it is beneficial for communicating with the emitter. For this reason, the mirror coating needs to be chosen to adequately balance these two factors taking into account the stability of the experiment.

How to measure the finesse of a given cavity will be derived in the following. Assuming a small φ, $\sin(\varphi/2) \approx \varphi/2$, and equation 2.11 can be written as

$$I = \frac{I_{\max}}{1 + (\mathcal{F}/\pi)^2 \varphi^2}. \tag{2.13}$$

The intensity decreases to half its maximum value if $\varphi = \pi/\mathcal{F}$ so that the full width at half maximum (FWHM) of each peak becomes

$$\Delta\varphi = \frac{2\pi}{\mathcal{F}}, \tag{2.14}$$

which is again manifestation that high finesse results in narrow peaks. But this is a FWHM of the peaks of the intensity plotted as the phase difference between waves. What we actually measure in the laboratory is the intensity as a function of frequency. To establish the relation between these, note that the phase of two different sinusoidal waves that can exist in the cavity is the argument of the sinus function, kz. Because the total length traversed at each round-trip is $2d$, the phase shift after each cycle is $\varphi = 2kd$. Plugging in the definition of the wavenumber and solving for ν gives

$$\nu = \frac{\varphi c}{4\pi d} \quad \Rightarrow \delta\nu = \frac{c}{4\pi d}\Delta\varphi = \frac{\nu_F}{\mathcal{F}}, \tag{2.15}$$

where we have used the result for $\Delta\varphi$. To find the finesse it suffices therefore to scan a frequency range, find the distances between which high intensities occur and divide this by the FWHM at one such intensity peak. If a laser with a certain frequency is coupled to the cavity, the length of the cavity needs to be varied instead, setting the requirement on the design to be able to travel at least $450\ \mathrm{nm}$ because the wavelength of the relevant Nd transition is $892\ \mathrm{nm}$. The FWHM of the peaks in the intensity plot as a function of cavity distance can also be used to infer the stability requirement. Similar to how equation 2.15 was shown, we have

$$\delta d = \frac{c}{4\pi\nu}\Delta\varphi = \frac{\lambda}{2\mathcal{F}}. \tag{2.16}$$

The lowest finesse that is planned to be used in the upcoming experiments is 600, which would yield $\delta d = 0.7\ \mathrm{nm}$. This small value justifies the care that was put into the design process as outlined in chapter 4.

Closely related to the finesse is the quality factor Q defined at a resonance frequency ν_0 as

$$Q = \frac{\text{resonance frequency}}{\text{FWHM of resonance}} = \frac{\nu_0}{\nu_F}\mathcal{F} = \frac{d}{\lambda/2}\mathcal{F}, \tag{2.17}$$

where equation 2.15 and 2.9 where used in that order. Because the same result can be derived by defining Q as

$$Q = 2\pi\frac{\text{stored energy}}{\text{energy loss per cycle}}, \tag{2.18}$$

these two definitions are equivalent. It is intuitive that placing an emitter inside a cavity, the interaction is higher when less energy is lost, i.e. the bigger the quality factor is. It will be shown later that this relationship is linear and will be referred to as Purcell enhancement. The ineffectiveness of simply increasing the cavity length to increase the quality factor, as equation 2.17 might imply, will then also be clear.

Cavities with spherical mirrors

When misaligning two planar mirrors, the rays are easily caused to leave the cavity. Having at least one spherical mirror reduces this sensitivity significantly. Placing the planar mirror at $z = 0$ (in the reference of figure 2.4) and the second mirror so that its radius of curvature r_c matches the radius of curvature of the Gaussian beam, it is easy to convince oneself why a Gaussian beam is a mode of such a cavity. But because of the identical wavefronts, also the Hermite Gaussian beams of order (l, m) are possible resonant modes. Because of the Gouy phase, the resonance frequencies now take the form

$$\nu_{l,m,q} = q\nu_F + (l + m + 1)\frac{\Delta\xi}{\pi}\nu_F = q\nu_F + (l + m + 1)\arccos\left(\sqrt{1 - d/r_c}\right), \quad (2.19)$$

where the last equality is not obvious but derived in [31]. If one wants to have a certain frequency, the mirrors still need to be spaced apart from each other at a certain distance. But because at this distance the wavefronts need to also match the mirror's radius, the latter needs to be engineered accordingly. The spherical mirrors for this work's cavities are build by laser ablation at an optical fiber's tip making it possible to change the radius of curvature on demand [11]. The resonator's eigenmodes then have their waist W_0 on the plane mirror [31].

A last characteristic of a resonator is its mode volume given by

$$V_m = \frac{\pi}{4}W_0^2 d \quad (2.20)$$

which is less than the volume of a cone with basis radius W_0. It is clear that if the mode volume is small, the energy is confined more densely. When an emitter is placed inside the cavity, its interaction with the cavity is stronger for smaller mode volumes. This explanation should serve as an intuition to the Purcell enhancement that will be introduced in section 2.3.

Fiber Fabry-Pérot cavities

Plane-concave cavities where the concave mirror is on the tip of a single mode fiber exhibit extremely good properties for both mode volume and qualiy factor. To achieve this, the fiber tip is made subject to CO_2-laser pulses resulting in approximately Gaussian surface profiles. Because these are so shallow, the mirrors can be brought together extremely close [33]. The extremely low roughness together with a high-performance dielectric coating account for the high quality factor and a finesse of up to 100 000. Additionally, small radii of curvature less than 10 µm keep the waist radius small giving mode volumes of a few λ^3. Emitters inside nano crystals can then be coated onto the planar mirror. Nanopositioners allow for spatial scanning as described more closely in section 3.3. A close up schematic of the two mirrors can be seen in figure 2.5

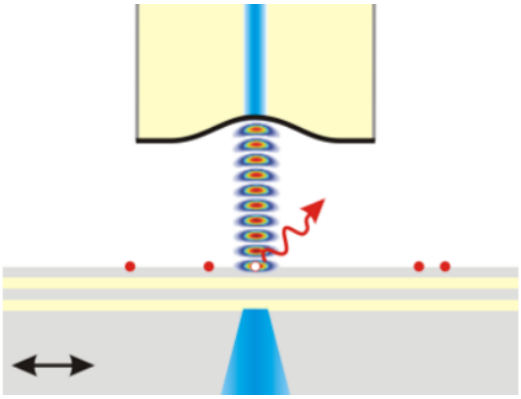

Figure 2.5: A schematic representation of a fibre Fabry-Pérot cavity consisting of a macroscopic plane mirror and a laser-machined fibre. Nanocrystals are applied to the macroscopic mirror. The mirrors can be moved with respect to each other in all directions. Figure taken from[32].

2.3 Cavity QED with rare earth ions

The rate at which REI quantum computer computations can be executed depends on how fast an ion can decay back to its ground state, its qubit's $|1\rangle$ state. This happens by spontaneous emission (SE), a slow process in free space. Nobel laureate Edwin M. Purcell proposed in his seminal 1946 paper that the SE rate of an atom is not an intrinsic property, but is modified when placed inside a resonant cavity [34]. An outline of how this statement can be arrived at is given in the appendix, summarizing the derivation given in [29] but skipping the detailed analysis found in [35].

It starts from explaining the quantum mechanical description of SE, a concept that is impossible to describe classically. Intuitively one could think that SE only depends on the energy levels of an atom, and that is true when the atom is in vacuumed free space. But similarly to the density of states for electrons in Solid State Physics, there exists a density of states for photons, altered when photons are restricted to the space of a cavity. Another concept of cavities is that emitted photons tend to re-excite the atom, and for a perfect cavity one observes a continuous oscillation between de-excited atom plus photon and excited atom.

In a lossy cavity, the electromagnetic decay rate decreases exponentially in time with decay rate $\Gamma_{cav} = \omega/Q$. If the losses are big enough, the system is in the weak coupling regime where the oscillation can no longer be observed but the decay rate $\Gamma_{sp,cav}$ is modified from the free space

decay rate, Γ_{sp}. It is enhanced when the cavity is resonant with a transition, and placing the atom in an antinode of the cavity mode leads to the ratio

$$\frac{\Gamma_{sp,cav}}{\Gamma_{cav}} = \frac{3}{4\pi^2}\frac{Q\lambda^3}{V_{mode}}, \tag{2.21}$$

referred to as Purcell factor. Thus, to improve enhancement of spontaneous emission the Q-factor needs to be maximum and the mode volume minimum, just as was mentioned earlier. But because the Q-factor increases with d and so does the volume, changing the cavity length has no overall effect. To increase the enhancement, it is therefore the finesse that needs to be increased.

3. Method

It was the aim of this thesis work to build a holder that puts together a planar mirror and a mirror coated fiber. This holder must be able to be inserted into a liquid helium cryostat which limits the dimensions for the design. The opening for the cryostat is circular with a diameter of $25\ \mathrm{mm}$. Having the holder at the end of a long metal rod, it can be inserted into the helium bath at the bottom of the cryostat. The pumping of the cryostat induces vibrations that could affect the cavity length. It is therefore required to build the setup with maximum passive stability. It is assumed that the induced vibrations will have a maximum frequency and maximizing the resonant frequencies of at least the individual parts is the strategy followed throughout. Another advantage of this approach is that a given vibrational energy results in smaller amplitudes for higher frequencies. Wanting to avoid differences in thermal expansion between parts, everything will be made out of titanium, the nanopositioners' material.

3.1 CAD software

The software chosen for designing the holder is SolidWorks , a solid modeling computer-aided design (CAD) program. Building a model in SolidWorks starts with a 2D drawing that can be extruded to create 3D models. Multiple models can then be added together in an assembly and positioned with respect to each other by mating operations.

The same program provides simulation options based on the finite element analysis (FEA). Instead of analytically solving the differential equations for heat transfer, the FEA reformulation of the problem consists of a system of algebraic equations that can be solved numerically. To do so, a model or assembly is subdivided into smaller parts called finite elements whose behaviour is governed by simple equations. These are then combined in a larger system of equations yielding approximate total solutions. There exist various types of simulations in SolidWorks but only the Frequency, the Static and the Linear Dynamic were exploited for this work. The first one of these yields the natural frequencies of the studied object. These should preferably

be as high as possible because it is then less likely that the vibrations will excite them. The Static simulation makes it possible to observe deformations under temperature changes which might lead to mirrors cracking under the contraction of their holders. Linear Dynamic studies give the response to a frequency spectrum, more precisely to the frequency components of a signal's power, the power spectral density (PSD).

3.2 CNC machining

The drills that will be used for fabricating the holder are computer numerically controlled (CNC). The CAD files can directly be uploaded to it and blank pieces of material can be altered to give the desired shape without a manual operator. Just like any other kind of drill, their minimum radius limits the sharpness of edges that can be achieved. The vertical corner radius at internal edges should therefore be minimally one third of the depth drilled but if even bigger, machining will be faster and more affordable. Walls should be at least half a millimeter thick and the diameter of holes should not be less than a millimeter but if threaded, they should be at least twice this size (fit for M2 screws). Drawings need to include a tolerance for which the standard tolerance for metal, $0.125\ \mathrm{mm}$, is chosen. In principle machining can happen from all sides, but if the shape can be achieved without rotating the material, costs will be reduced. Metal is usually sold in a variety of shapes, rods being the most economic version for titanium. Because the cryostat insertion hole is circular, this is a fortunate coincidence and is further exploited in the very last design. It was part of the thesis work to communicate with external workshops for the fabrication, and quotations were requested from Sweden, Germany and Switzerland.

3.3 Scanning the cavity

Scanning the cavity horizontally to find the crystals on the substrate and vertically to bring the cavity to resonate with an atomic transition will be done by attocube's nano positioner line ANP51. Enough of these are already owned by the Quantum Information group and they have been shown to work for this application [32]. They are small (surface area of $15\ \mathrm{mm} \times 15\ \mathrm{mm}$) but the set up size is limited by the cryostat opening anyway. The limit they really introduce is the weight they can carry. Each horizontal attocube can only be loaded with $25\ \mathrm{g}$ [36] and because they each weighs $7\ \mathrm{g}$, the construction on top of two stacked attocubes may not exceed $18\ \mathrm{g}$. The vertically moving attocube can take twice as much weight, a limit far from being reached. This z-attocube will eventually be used to bring the fiber close to the substrate whereas an additional small shear piezo will be used in scanning the length of the cavity.

4. Results

4.1 Design steps

The design was continuously improved during numerous group meetings, dedicated discussions and conversations with individual group members. Nevertheless, four major revisions can be identified and are described here together with their associated strengths and weaknesses. The three first core ideas are represented also in figure 4.1.

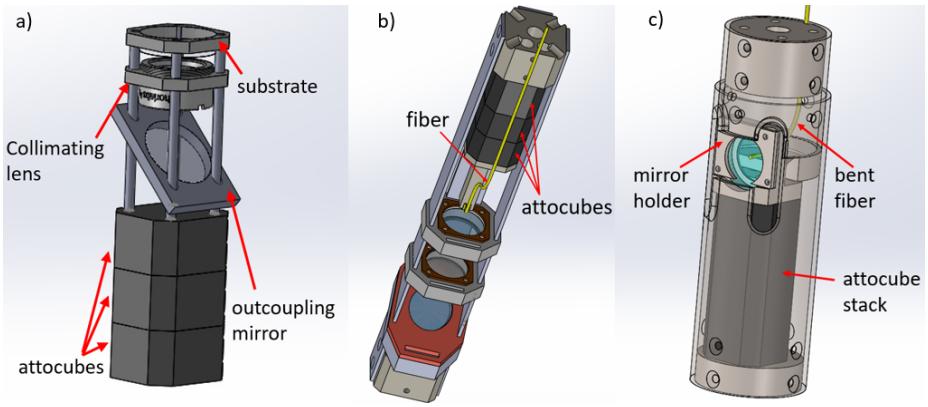

Figure 4.1: The three first design proposals. a) The moving part of the first design where the fiber would approach the substrate from above (the fiber and the rest of the cage is not seen here). b) The fiber as the moving component of the set up. c) The fiber bent 90° inside a cylindrical cage.

The first step in the design was to stack three attocubes, as can be seen in figure 4.1 a, and to mount them on a circular base plate. An outcoupling mirror, angled at 45 degrees with respect to the horizontal, was then sandwiched between the attocubes and the substrate. These two mirrors would then move together to scan horizontally and also in the vertical directions to approach the mirror coated fiber hanging from the top. Actually, the first designs also included a collimating lense inside the cryostat between the outcoupling mirror and the substrate. This long construction, held on top of three attocubes by some sort of framework, would of course not be very stable. It was therefore verified that the collimating lense could be placed outside the cryostat. For this to be possible, the beam's width should not be bigger than the window through which it can leave. Assuming an initial beam waist of 2 µm and the distance between substrate and window to be 17 cm, $W(z, \lambda)$ can easily be computed by combining the formulas given in the first and third point explaining the Gaussian beam (equation 2.7). The relevant wavelengths, having values below 900 nm, result in a width of less than 30 mm, well below the

window's radius. A structure with the collimating lense outside the cryostat is therefore feasible and is close to what stands as the final design. Before this one could be decided upon, a few other concepts were considered.

A second design switched the moving part. Here, the fiber, still hanging, was the part of the cavity that moved in all three directions. For that purpose, also all the attocubes had to be hanging, a method inspired by a paper on an entirely different application [37]. According to attocube's customer service the same specs on the loading apply also in this configuration. For the fiber to be centralized, a relatively long dedicated holder had to be designed as can be seen in figure 4.1 b. In order to avoid this and the outcoupling mirror, this model was completely revisited though.

In this revised version the fiber does not hang straight down any longer but is bent $90°$ and the substrate is held vertically by a special holder (see figure 4.1 c). However, the particular fibers relevant to our setup do not allow for the sharp bending radius of $10\ \mathrm{mm}$, and this method had to be abandoned. Having the least tower like structure of all the designs, it would have probably been the most stable one and it is no wonder that other groups use similar constructions [32].

The fourth and final design then combined the feedback collected from all previous steps. In fact, it is a combination between the first two designs. To avoid high towers as much as possible, the horizontal attocubes were now detached from the vertical attocube so that the fiber could still be moved vertically but horizontal scanning would happen by the substrate.

After an initial sketch, this was designed in a way so that it could be manufactured easily by CNC machines, fulfilling all the requirements mentioned in section 3.2. The outcoupling mirror will have to be glued in its holder because there was no space for screws. This design was then 3D printed and a quote was received by a German manufacturer. From the 3D print and the manufacturer's feedback it was then decided to increase the thickness of certain parts. This was done by starting from cylindrical blocks and then virtually milling them to the desired shapes. In this way, they would fit perfectly into the outer cylinder of the holder and would be produced easily. Its CAD model can be seen in figure 4.2.

What this design also includes is a locking mechanism: once the fiber is in place, a third x-attocube attached sideways parallel to the fiber ("locking attocube" in figure 4.2) can be extended once the fiber is in a correct position. It then presses onto the substrate so that vibrations would only make the fiber and the plane mirror swing in the same direction, the fiber is hence "locked" to the substrate. For further horizontal scanning it can be moved inward before it relocks again. Simulations were performed with the goal to find a qualitative difference between a system that uses this locking mechanism and one that does not. As it turned out, the locked set up was to difficult too properly simulate but the efforts of trying to achieve that goal are described below alongside other simulation results.

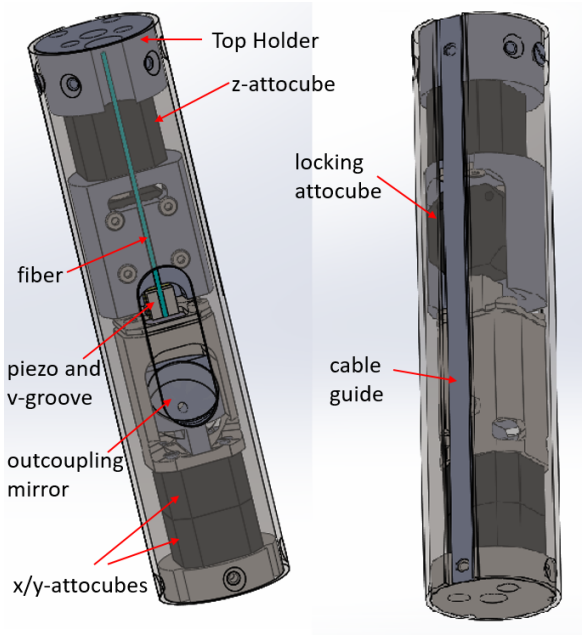

Figure 4.2: The final CAD design for the cryostat holder. Everything apart from the mirrors, the fiber and the piezo will be made out of titanium; the color code is only used for clarification and the outer cylinder is transparent only to allow observation of all pieces. The length of the whole assembly is 104 mm.

4.2 Simulations

Simulating the thermal expansion of interfaces between glass and metal is the easiest study carried out for this thesis. SolidWorks only calculates behaviour assuming a constant coefficient of expansion but this leads to conservative estimates because as the temperature drops below 200 K, the coefficient of relevant metals and fused silica drops to zero and eventually below that, before it increases again to zero towards 0 K [38, 39, 40]. The substrate material, fused silica, has a very low coefficient of thermal expansion and in the simulations it is suppressed even further to 1×10^{-8} K^{-1}. For titanium this coefficient is taken to be 9×10^{-6} K^{-1} and for stainless steel 1.6×10^{-5} K^{-1}. The latter is included only for comparison.

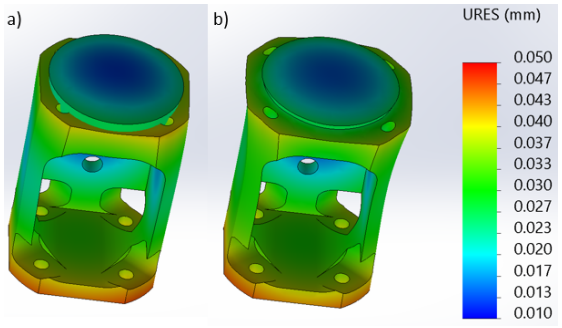

Figure 4.3: The contraction of the mirror holder at 2.17 K with a hole diameter of a) 12.8 mm and b) 12.7 mm. In a) it seems as if the holder sinks into the mirror but that is only because the deformation is exaggerated.

A metal part enclosing a fused silica mirror must be so far apart from it as to not put more than 1130 MPa of pressure on the mirror upon contraction [41], but the simulated stress put

onto the substrate might not reflect the actual values once in the cryostat. A simpler way of guaranteeing that the glass does not crack is to simulate whether a mirror holder would contract to $12.7\ \mathrm{mm}$ because this conclusion does not rely on material strength assumptions. By this approach we conclude that a stainless steel mirror holder should have a diameter of $12.9\ \mathrm{mm}$, made out of titanium, $12.8\ \mathrm{mm}$ is enough. For completeness, the pressures onto the mirror at changing hole diameters of different materials are summarized in table 4.1. According to them, even a $12.7\ \mathrm{mm}$ hole would have been enough, but this simulation assumes certain material behaviour that might be different at cryogenic temperatures.

Table 4.1: SolidWorks simulation for thermal contraction at $2.17\ \mathrm{K}$ for different materials, mirror holder diameters and corresponding pressures onto the substrate (with compressive strength of $1130\ \mathrm{MPa}$).

material	holder diameter (mm)	pressure on glass (MPa)
steel	12.7	820
	12.8	550
	12.9	360
titanium	12.7	400
	12.8	330
	12.9	290

Simulating the vibratory response is slightly more involved, requires more assumptions and is less quantitatively reliable because the attocubes were just simulated as if to behave like solid blocks. For cryogenic insertion, the cryostat holder will eventually be screwed to the end of a long metal rod. Including this in the model, and applying a time varying force onto some part of the holder will preferably bring the rod into a swinging motion instead of showing how the holder itself reacts. Similarly, when the natural frequencies are simulated, the first ones basically only show how the rod swings in different ways. A more interesting assumption is therefore that the top of the holder be fixed. This could be achieved by either fixing the top surface or the surface inside the threaded hole used to connect to the metal rod. Interestingly enough, this makes quite a difference for the first natural frequencies as can be seen in table 4.2. Because the latter way of fixing seems more natural, it was chosen for most of the coming analysis.

The simplest simulation for reaction to imposed forces is a static one. Applying a certain force on any part of the holder, one could observe how any other part of it moved. The points of interest were chosen to be the center of the substrate (other spots on the substrate being more difficult to probe) and the spot where the fiber tip would lie. These would not be facing each other directly but since what is measured is the distance which each point moves, any point on the substrate should work equally well. When a force of $1\ \mathrm{N}$ is applied on the bottom of the holder, fixed on the top surface, the substrate would move more than the fiber by $60\ \mathrm{nm}$. This is the difference of the magnitude of the two vectors that are spanned between each probe's point before and after excitation. Often, these vectors are labelled with U and are a *resultant* of the displacement. Their magnitudes are therefore often referred to as $URES$. But, even if the two points have travelled the same distance, they could have done so in opposing directions. It is

Table 4.2: The first five simulated natural frequencies for a set up close to the final one. Different results are obtained depending on the holder's fixture.

Mode No.	Frequency when top surface is fixed (Hz)	Frequency when top hole is fixed (Hz)
1	1142.5	1142.2
2	1145.2	1142.9
3	3023.3	3008.6
4	3633.5	3631.6
5	3704	3701

nonetheless better to have two vectors of similar magnitude and if possible, to minimize these. Again, this analysis is not to be interpreted quantitatively but can be meaningful in comparing to other configurations or set ups.

A yet more interesting simulation is to apply a time varying force which could be done by executing a Linear Dynamic Study, taking a PSD as input. How exactly the PSD of the cryogenic vibrations for our laboratory looks like is not known and a random PSD was used. This should include at least the first five natural frequencies and go to zero at the origin. Using always the same PSD, it should then be possible to compare the quality of different set ups. The curve used here is square root function like with a y-value of 90 (in not specified units) at the fifth's mode (3701 Hz, see table 4.2). The result can be seen in figure 4.4, visualized at the fifth frequency and its displacement vectors plotted over all input frequencies, over which the difference in the length of the displacement vectors remains approximately around 0.01 nm. It can be seen that the magnitude of both vectors decreases with increasing frequency, and that they do approach each other slightly even though the intensity at higher frequencies increases. This behaviour is rather linear and no peaks are observed around the resonance frequencies. It was then also tested how the system reacts to signals whose PSDs each peak at one of the resonance frequencies and is zero otherwise, but the result is similar to the one obtained by having the PSD ranging over more frequencies.

What this should have been compared to, is the same set up but with the locking mechanism in place. The idea was to contact the locking attocube to the substrate holder as described in section 4.1. SolidWorks in principle has the option of letting two touching surfaces be moved along each other with a certain coefficient of friction between them. Unfortunately, this option is not available in the Linear Dynamic Study. A study with this option is called Nonlinear Study, but this one cannot take PSDs as an input, instead relying on time spectra. Certainly, a PSD covering many frequencies would result in an extremely complicated time spectra which in turn makes computations very heavy. It was tried nonetheless to convert the previously used PSD into such a time signal, and a reduced model of the set up was used. Exhibiting rotational symmetry, this reduced model should reduce calculations significantly. Despite this effort, all the simulations failed. Converting a PSD signal only consisting of delta functions around the natural frequencies into a time signal proved equally unsuccessful. It is still believed that a locking mechanism benefits the stability, but one issue that it introduces is that it increases the size of the set up. The design was therefore modified to be able to include one version with and

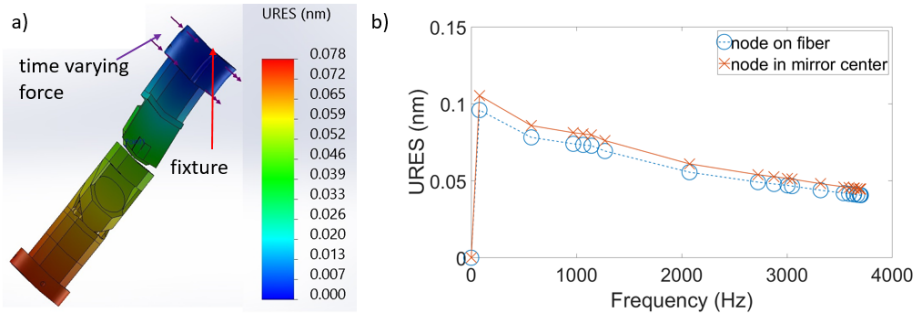

Figure 4.4: a)An exaggerated view of how the holder reacts when a time dependent force is applied. This is the shape at the fifth natural frequency, 3701 Hz. b) The magnitude of the displacement vectors as a function of frequency up to the fifth natural frequency value. One displacement vector corresponds to a node set in the center of the substrate, the other to a note set on the fiber tip's position.

one without the locking. Going from one to the other only requires changing one piece and fixing the top part differently.

4.3 Construction and materials

To test how the design could be handled in practice, the second to last design was 3D-printed. The result can be seen in figure 4.5 and the conclusion from this prototype was, as previously mentioned, to increase certain wall thicknesses further. It could be confirmed that assembling everything poses no problem.

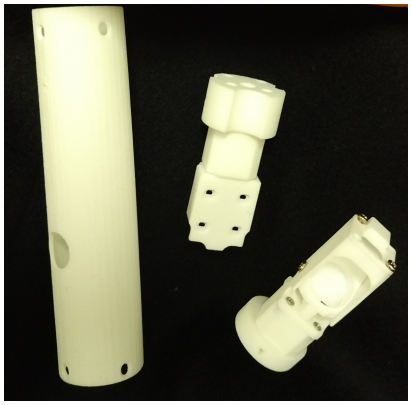

Figure 4.5: The 3D printed outer cylinder next to the top part eventually holding the fiber and the bottom part (here with only one horizontal attocube).

The fibers that constitute one side of the cavity are bought on a roll of 700 m and are thus not connectorized. Cut into a few meter long pieces, they will be able to leave the cryostat where light from a laser is supposed to be coupled into them. The laser light for the coming experiments is already coupled into an optical fiber with FC/APC connectors (the FC refers to the type of ferrule and the APC means that the fiber endface is polished at an 8-degree angle). It would therefore be easiest to also have such connectors on the cavity fibers. One option for achieving this would be to fusion splice the end of the fiber to a patch cable already equipped with a connector. But because fusion splicers are very expensive and standard patch cables are doped with germanium, possibly fluorescing, it was decided to connect the fibers to the appro-

priate connectors by epoxy and then polish the fiber endface to $8°$. An appropriate termination kit was ordered from Thorlabs [42].

A last product that had to be bought is the shear piezo for fine tuning of the cavity length. Its requirements are to have a high travel range (ideally more than a FSR, $450\ \mathrm{nm}$) at cryogenic temperatures and to be as compact as possible. The PL5FBP3 version from Thorlabs seemed to be the best option. It is equipped with aluminum end plates and leads, facilitating electrical connections. These extra features make the piezo more than three times as thick as their simpler versions, but they are still thinner than the ones offered by competitors and fit into the design. Their travel range of $1.3\ \mu\mathrm{m}$ will probably be reduced to $130\ \mathrm{nm}$ at $2.17\ \mathrm{K}$, better than other similar products, and that at lower cost. To cover the whole FSR, the z-attocube might be used additionally.

5. Conclusion and Outlook

While not yet built, the final design for the cryostat holder has been achieved and the order for its manufacturing is ready to be placed. The simulation for comparing locked and not locked systems has been proven to be inaccessible with SolidWorks but numerous other small simulations were used to increase the resonance frequency of individual parts. It might be possible to achieve a simulation for the locked system if only simple sinusoidal functions are used for the time dependent signal. These could then be repeated for all relevant frequencies. But how to determine the relevancy of a frequency is still a remaining question because it is unknown which vibrations the cryostat actually induces. An accelerometer could be used to find these and is about to be bought. A 3D print helped in determining certain weaknesses and also proved that assembling the system poses no difficulties.

For manufacturing the actual holder in titanium, several workshops were consulted and quotations were received. It is now only some weeks left to wait before the holder can be tested and used for (hopefully) single ion detection. All other components are already ordered for that purpose. These include the custom made fibers (for which a time for coating them is already scheduled), the connectorization set, the shear piezo, the glue and all necessary screws.

Some initial testing should be done on the holder's resonance frequencies and vibratory behaviour. Setting it up to function as a resonant cavity without emitters, one could simply induce controlled vibrations and observe the effect they have on the out-coupled light.

How the light should be coupled out of the cavity is also still to be determined. An obvious approach would be to look at what is coupled out of the cryostat window, but it is also possible to detect the light that couples from the cavity back into the fiber. For this to work, one would have to use a specific adapter that is not available out of the same material as the cavity fiber. Because this adapter could induce fluorescence it might be difficult to use this method when wanting to detect single ions. The advantage of this method would be that the light is already coupled into a fiber, simplifying the analysis.

Testing the whole set up inside the cryostat will be the most important step because it is only

there that meaningful qubit interactions are possible. It would actually surprise me if everything worked without problems but I believe that the proposed set up is able to undergo modifications without having to reproduce the whole part. A possible modification could be to introduce another locking mechanism, maybe using piezos instead of the attocube. This would need extreme precision in the initial alignment and is not feasible for now. Should it become possible, it will easily be able to be implemented in this holder.

Other pieces that still need to be built are a jig to hold the set up in place while it is being assembled and a dedicated cryostat rod. The latter is important because other experiments run at the same time and it is impractical to disassemble the whole set up all the time. And even if such a rod will not be built soon, what needs to be built as soon as possible is an adapter for the current rod. At the moment it screws directly into the holder, meaning that either the holder or the rod have to be turned around its axis which might break the cables or even the optical fiber.

Apart from testing the holder's resonance frequencies, I propose to measure the finesse of the cavity early on in order to get used to handling the scanning method. First, the cavity should be set to an arbitrary length and the frequency be varied in order to determine the finesse as described earlier on. This can then be repeated at several horizontal positions of the substrate. Once this is successful, the cavity should be brought to a position that is resonant with the relevant Nd transition and then varied around that position. If both work, it would already be a huge step towards Purcell enhancement and finally single ion detection.

I started writing this thesis with these last experimental steps in mind. The theoretical section is used to motivate the reason for constructing the set up and to justify certain design considerations. Being the first thesis project using a fiber Fabry-Pérot cavity in Lund, my thesis includes a rather extensive summary of the relevant concepts and I hope that it will, together with the references, be useful for future Bachelor or Master projects.

Bibliography

[1] P. Shor. Polynomial-time algorithms for prime factorization and discrete logarithms on a quantum computer. *SIAM Journal on Computing*, 26(5):1484–1509, 1997.

[2] Fernando Pastawski, Norman Y. Yao, Liang Jiang, Mikhail D. Lukin, and J. Ignacio Cirac. Unforgeable noise-tolerant quantum tokens. *Proceedings of the National Academy of Sciences*, 109(40):16079–16082, 2012.

[3] T. D. Ladd, F. Jelezko, F. Jelezko, R. Laflamme, Y. Nakamura, C. Monroe, and J. L. O'Brien. Quantum computers. *Nature*, 464:45–53, 2010.

[4] Nicklas Ohlsson, R Krishna Mohan, and Stefan Kröll. Quantum computer hardware based on rare-earth-ion-doped inorganic crystals. *Optics Communications*, 201(1):71 – 77, 2002.

[5] C.W. Thiel, Thomas Böttger, and R.L. Cone. Rare-earth-doped materials for applications in quantum information storage and signal processing. *Journal of Luminescence*, 131(3):353 – 361, 2011. Selected papers from DPC'10.

[6] Manjin Zhong, Morgan P. Hedges, Rose L. Ahlefeldt, John G Bartholomew, Sarah E. Beavan, Sven Wittig, Jevon Longdell, and Matthew J. Sellars. Optically addressable nuclear spins in a solid with a six-hour coherence time. *Nature*, 517:177–180, 2015.

[7] Utikal, Eichhammer, Petersen, Renn, Götzinger, and Sandoghdar. Spectroscopic detection and state preparation of a single praseodymium ion in a crystal. *Nature Communications*, 5, 2014.

[8] Kolesov, Xia, Reuter, Stöhr, Zappe, Meijer, Hemmer, and Wrachtrup. Optical detection of a single rare-earth ion in a crystal. *Nature Communications*, 3, 2012.

[9] A. Perrot, Ph. Goldner, D. Giaume, M. Lovrić, C. Andriamiadamanana, R. R. Gonçalves, and A. Ferrier. Narrow optical homogeneous linewidths in rare earth doped nanocrystals. *Phys. Rev. Lett.*, 111:203601, Nov 2013.

[10] D. Hunger, C. Deutsch, R. J. Barbour, R. J. Warburton, and J. Reichel. Laser microfabrication of concave, low-roughness features in silica. *AIP Advances*, 2(1):012119, 2012.

[11] D. Hunger, T. Steinmetz, Y. Colombe, C. Deutsch, T. W. Hänsch, and J. Reichel. A fiber fabry–perot cavity with high finesse. *New Journal of Physics*, 12(6), 2010.

[12] M. Mader, J. Reichel, T. W. Hänsch, and D. Hunger. A scanning cavity microscope. *Nature Communications*, 6:7249, 2015.

[13] Hanno Kaupp, Christian Deutsch, Huan-Cheng Chang, Jakob Reichel, Theodor W. Hänsch, and David Hunger. Scaling laws of the cavity enhancement for nitrogen-vacancy centers in diamond. *Phys. Rev. A*, 88:053812, Nov 2013.

[14] Roland Albrecht, Alexander Bommer, Christian Deutsch, Jakob Reichel, and Christoph Becher. Coupling of a single nitrogen-vacancy center in diamond to a fiber-based microcavity. *Phys. Rev. Lett.*, 110:243602, Jun 2013.

[15] Erika Janitz, Maximilian Ruf, Mark Dimock, Alexandre Bourassa, Jack Sankey, and Lilian Childress. Fabry-perot microcavity for diamond-based photonics. *Phys. Rev. A*, 92:043844, Oct 2015.

[16] Hümmer, Noe, Hofmann, Hänsch, Högele, and Hunger. Cavity-enhanced raman microscopy of individual carbon nanotubes. *Nature Communications*, page 043844, Jul 2016.

[17] Bernardo Casabone, Julia Benedikter, Thomas Hümmer, Franziska Beck, Karmel de Oliveira Lima, Theodor W. Hänsch, Alban Ferrier, Philippe Goldner, Hugues de Riedmatten, and David Hunger. Cavity-enhanced spectroscopy of a few-ion ensemble in eu3+:y2o3. *New Journal of Physics*, 20, 2018.

[18] Michael A. Nielsen and Isaac L. Chuang. *Quantum Computation and Quantum Information*. Cambridge University Press, 2000.

[19] Aram W. Harrow and Ashley Montanaro. Quantum computational supremacy. *Nature*, 549:203–209, 09 2017.

[20] Austin G. Fowler, Matteo Mariantoni, John M. Martinis, and Andrew N. Cleland. Surface codes: Towards practical large-scale quantum computation. *Phys. Rev. A*, 86:032324, Sep 2012.

[21] Richard P. Feynman. Simulating physics with computers. *International Journal of Theoretical Physics*, 21(6):467–488, Jun 1982.

[22] Boris Korzh, Charles Ci Wen Lim, Raphael Houlmann, Nicolas Gisin, Ming Jun Li, Daniel Nolan, Bruno Sanguinetti, Rob Thew, and Hugo Zbinden. Provably secure and practical quantum key distribution over 307 km of optical fibre. *Nature Photonics*, 9:163–168, February 2015.

[23] Do bacteria and dna adsorb rare earth elements? opening the door to application from atomic-level viewpoint. `http://www.spring8.or.jp`. Accessed: 2018-10-12.

[24] Uyugun Vakhidovich Valiev, John B. Gruber, and Gary W. Burdick. *Magnetooptical spectroscopy of the rare-earth compounds: development and application*. Scientific Research, 2012.

[25] A. J. Freeman and R. E. Watson. Theoretical investigation of some magnetic and spectroscopic properties of rare-earth ions. *Phys. Rev.*, 127:2058–2075, Sep 1962.

[26] Anthony E. Siegman. *Lasers*. University Science Books, 1986.

[27] Bahaa E A Saleh and Malvin Carl Teich. *Fundamentals of photonics; 2nd ed.* Wiley series in pure and applied optics. Wiley, New York, NY, 2007.

[28] Sébastien Forget. Optical resonators and gaussian beams. `http://www.optique-ingenieur.org/en/courses/OPI_ang_M01_C03/co/Contenu_08.html`. Accessed: 2018-10-12.

[29] Gilbert Grynberg, Alain Aspect, and Claude Fabre. *Introduction to quantum optics: from the semi-classical approach to quantized light*. Cambridge Univ. Press, New York, NY, 2010.

[30] F.L. Pedrotti and L.S. Pedrotti, L. M. anPedrotti. *Introduction to Optics*. Prentice Hall, 2008.

[31] Nicolas Barré, Marco Romanelli, M Lebental, and Marc Brunel. Waves and rays in plano-concave laser cavities: I. Geometric modes in the paraxial approximation. *European Journal of Physics*, 38, 2017.

[32] Franziska Beck. Europium-doped nanocrystals in cryogenic optical microcavities. Master's thesis, Ludwig-Maximilians-Universität München, 2016.

[33] D. Hunger, T. Steinmetz, Y. Colombe, C. Deutsch, T. W. Hänsch, and J. Reichel. A fiber fabry–perot cavity with high finesse. *New Journal of Physics*, 12(6):065038, 2010.

[34] E. M. Purcell. Spontaneous emission probabilities at radio frequencies. volume 69, pages 681+, 1946.

[35] Serge Haroche and Jean Michel Raimond. *Exploring the Quantum: Atoms, Cavities, and Photons*. Oxford Univ. Press, Oxford, 2006.

[36] attocube systems AG. *ANPx51 Technical Specifications*, 2018.

[37] M. Tortello, W. K. Park, C. O. Ascencio, P. Saraf, and L. H. Greene. Design and construction of a point-contact spectroscopy rig with lateral scanning capability. *Review of Scientific Instruments*, 87(6):063903, 2016.

[38] G K White. Thermal expansion of reference materials: copper, silica and silicon. *Journal of Physics D: Applied Physics*, 6(17):2070, 1973.

[39] S.J. Collocott and G.K. White. Thermal expansion and heat capacity of some stainless steels and feni alloys. *Cryogenics*, 26:402–405, 07 1986.

[40] Van Sciver and Steven W. *Helium cryogenics; 2nd ed.* International cryogenics monograph series. Springer, New York, NY, 2012.

[41] TOSOH USA, Inc. *Fused Silica Glass*, 2013.

[42] Thorlabs, Inc. *FN96A, Guide to Connectorization and Polishing Optical Fibers*, 2018.

[43] Adam Kinos. *Light-Matter Interaction and Quantum Computing in Rare-Earth-Ion-Doped Crystals*. PhD thesis, Lund University, 2018.

[44] John David Jackson. *Classical electrodynamics*. Wiley, New York, NY, 3rd ed. edition, 1999.

Appendices

A. A rare earth ion C-Not gate

This appendix provides the details in how to create a C-Not gate with rare earth ions. Considered the simplest two qubit gate, it is explained here in detail for the reader interested in Quantum Computing with rare earth ions but it is not needed to understand the main part of the thesis.

It is assumed that the ions in question have three hyperfine levels and that these are equally populated at cryogenic temperatures. To get a pure quantum state, optical pumping can continuously excite the electrons from the higher lying levels to an excited state. After this, the ions will conserve their state for a very long time due to the unusually long lifetimes of the hyperfine levels. Having multiple qubits in a crystal, they only differ in their energy of the optical transition, with the absorption frequency corresponding to the $|0\rangle$ to excited state transition. What stays constant, is the splitting between the two states of a qubit.

While the permanent dipole moments between the hyperfine levels do not differ, when going from the ground state to an excited state, the permanent dipole moment changes. Hand in hand with this change goes an electrical field change, big enough so that neighbouring ions are sensitive to it. This results in their frequencies being shifted just as they were shifted already by lattice imperfections. Because of this effect, controlled logic between different qubits can be performed. A constraint is that a laser used to excite the unperturbed ions, has no effect on the shifted ions anymore. This implies a necessary shift of a few linewidths. That way, interactions between ions only occur when it is decided to excite an electron from one of the qubit states to an excited state. For he rest of the time one can perform single qubit operations without being perturbed by other ions. The necessary pulse sequences are explained in the next paragraph and are depicted in figure A.1

The physical control qubit in this set up is an ion j. After optical pumping, a pulse that would excite the control qubit's $|0\rangle$ state is applied. If ion j was in the $|0\rangle$ state, the transition is successful and the change in dipole moment is felt by the target ion i, shifting its frequency. Applying other pulses that correspond to the i^{th} ion's original absorption frequency can only succeed if the ion did not experience an electrical field change resulting from the control ion's excitation. If successful, the target ion will eventually decay to its $|1\rangle$ state. Because of the frequency shifting, this population transfer only happens if the control ion was originally in its $|1\rangle$ state. It is apparent that this is just as the theoretical controlled-NOT gate described in the theory section. In conventional crystals, many ions respond to the same frequency and laser beams cannot be focused so to only contain one ion. The ions are then also so far from each other that their dipole transitions will not be felt anymore by all other ions. It is still possible to implement a controlled-NOT gate in this scenario but more auxiliary steps are required [4].

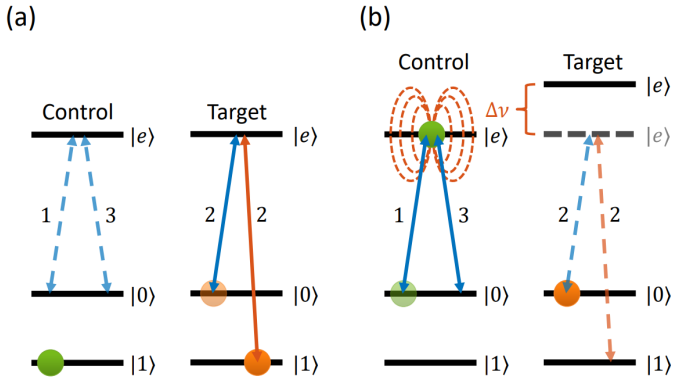

Figure A.1: C-Not pulses that are applied to the qubits can result in excitation and de-excitation if resonant with a transition and are denoted by the numbered arrows associated with the transition. If the arrow is dashed, the applied pulse does not lead to any transition. (a): The control is in $|1\rangle$ and is unaffected by the first pulse (1) which makes the second pulse sequence (2) on the other qubit effective and the third pulse (3) ineffective. (b): The control is in $|0\rangle$, making (1) effective and therefore shifting the target qubit's energy level so to make (2) ineffective. (3) is effective in this scenario. Figure taken from [43].

B. Interaction of an atom with the quantized electromagnetic field

While Purcell enhancement can simply be accepted as the equation given in the theory section, it is actually possible to derive it requiring only the Quantum Mechanics taught at an undergraduate level. This appendix outlines the derivation, but again, it is not needed to understand the rest of the thesis.

It turns out that spontaneous emission is a purely quantum mechanical concept and when describing the phenomena by means of classical physics, no sensible results can be obtained. The theoretical development in the language of quantum mechanics, on the other hand, gives results precisely in agreement with experiment. Classical literature (such as [27] used for the main part of the thesis) must therefore be abandoned to instead consult quantum optics textbooks (like [29] used for this appendix).

To see how en emitter acts when inside a field, we consider the total energy of the system (comprising both the emitter and the field). This can be written in a Hamiltonian form and be decomposed in a radiation Hamiltonian, a particle Hamiltonian (the one associated with the simple atomic model only involving Coulomb interaction, ignoring relativistic effects) and the interaction Hamiltonian:

$$H = H_R + H_P + H_I. \tag{B.1}$$

This also holds true in a classical world such as described by [44] but can be transferred to the operator formalism by appropriate changes. The momentum vector $\boldsymbol{p}$, found in the particle Hamiltonian to account for the electrons' motion around the nucleus, is for instance replaced by $\hat{p}$. The resulting Hamiltonian is thus precisely as in B.1, but with hats denoting the operator notation on every H. Assuming that the electromagnetic field does not vary much over an atomic range (long-wavelength approximation), $\hat{H}_I$ simplifies significantly. When the nucleus can be considered at rest, this interaction Hamiltonian can be written as the sum of two Hamiltonians, each responsible for different effects. The second one, $\hat{H}_{I,2}$, only contains terms that affect the radiation without changing the atomic state and will not be considered in the following. The first one, $\hat{H}_{I,1}$, is linear in the step operators ($H_{lI1} \propto \hat{a}_l$ and $\hat{a}_l^\dagger$). From perturbation theory we know that it therefore can only induce transitions that either add or subtract a photon to the electromagnetic field, corresponding to emission and absorption.

At this point, we need to introduce a bit of notation. An ensemble with an atom in state $|i\rangle$ and hit by n_1 photons in mode 1, ... n_l photons in mode l is denoted by $|i; n_1, ..., n_l, ...\rangle$. If all but one photon mode is present, one can write the total state by $|\phi_i\rangle = |\phi_i\rangle = |a; n_j\rangle$ where the atom is in state $|a\rangle$. This can be shown to be an eigenstate of $\hat{H}_P + \hat{H}_R$ which leads us to treating H_I as a perturbation. Under its effect, the system can either evolve to $|\phi_a\rangle = \left|b; n_j' = n_j - 1\right\rangle$ or $|\phi_e\rangle = |\phi_i\rangle = \left|c; n_j' = n_j + 1\right\rangle$ (because of the step operators). These are associated with absorption and emission of a photon and are also eigenstates of $\hat{H}_P + \hat{H}_R$. A perturbation can induce a transition between two eigenstates of the unperturbed Hamiltonian only if the two states have the same energy (this is actually only the most probable case, but the statement basically holds because of how unlikely the other cases are). We must therefore have $E_b = E_a + \hbar\omega_j$ (or $E_c = E_a + \hbar\omega_j$). With ω_j denoting the photon's wavelength, this is the standard result taught in elementary quantum mechanics courses ignoring perturbation theory. Another result, because $\hat{a}_j |n_j\rangle = \sqrt{n_j} |n_j - 1\rangle$, is that $\langle b; n_j - 1| \hat{H_I} 1 |a; n_j\rangle^2 \propto n_j$. Its interpretation is that the transition probability is proportional to the number of photons, i.e. the wave intensity, a rather logical result. Similarly, using the relation $\hat{a}_j^\dagger |n_j\rangle = \sqrt{n_j} |n_j - 1\rangle$, for emission $\langle c; n_j + 1| \hat{H_I} 1 |a; n_j\rangle^2 \propto n_j + 1$. This is interesting because it tells us that even with no incident photons ($n_j = 0$), the transition amplitude is non-zero. This process is called spontaneous emission (the other case being called stimulated emission). If there is another mode populated, say n_l, but n_j is not, then the atom will prefer to emit photons to mode l which is what makes a laser amplifier work.

An atom having emitted a photon can absorb another photon of the same wavelength to return to its original state. The radian frequency with which this change can happen back and forth is called the Rabi angular frequency, Ω_1, and will be used later.

An atom in vacuum, on the other hand, does frequently undergo spontaneous emission without reabsorption. It seems reasonable that it can emit photons of wavelengths varying only as a function of the energy state differences of the atom. In other words, discrete levels are coupled to a continuum. In this case Fermi's golden rule, telling us about the transmission probability Γ of a transition, applies:

$$\Gamma = \frac{2\pi}{\hbar}|W_{fi}|^2\rho_f, \tag{B.2}$$

where W_{fi} is the coupling matrix element and ρ_f is the density of final states. The latter can be found, just as is done for electrons confined in a material in solid state textbooks, by using the periodic boundary conditions for a cubic discretization volume of side L:

$$\rho_f = \left(\frac{L}{2\pi}\right)^3 \frac{E^2}{(\hbar c)^3}, \tag{B.3}$$

where E is the photon energy. In free space, L can be let go to infinity and the density represents a real continuum. In a cavity, this is not possible, and the quantization volume has actual physical meaning.

The take home message so far is that spontaneous emission is a joint property of the atom and the vacuum. The rate of spontaneous emission cannot be calculated without the full quantum formalism, even though only a small fraction of it was presented here. Without it, this joint property would not have emerged from theory. How this is used in practice, by effectively changing the atom's environment, shall conclude the appendix.

The most obvious cavity QED experiment one can do is to place an atom inside a cavity that is resonant with a certain atomic transition. The initially excited atom could decay and then reabsorb the circulating photon in the cavity. It can be shown that this behaviour is actually sinusoidal. If, on the other hand, the cavity is not resonant with any atomic transition, the atom will most likely remain in its original state.

Another, more realistic situation is the application of a Fabry-Pérot cavity with losses. The electromagnetic energy inside an empty cavity would decrease exponentially in time, with a decay rate $\Gamma_{cav} = \omega/Q$. A detailed analysis [35] shows that the system can evolve in two different ways:

- $\Gamma_{cav}/2 < \Omega_1/\sqrt{n_j}$: **strong coupling regime**
  With small losses, the probabilty of finding the atom in its excited state still oscillates but is damped now with Γ_{cav}.

- $\Gamma_{cav}/2 > \Omega_1/\sqrt{n_j}$: **weak coupling regime**
  Just like in free space, the excited state population decreases monotonically without oscillation. Its decay rate is modified with respect to the free space decay rate Γ_{sp}, and can be enhanced when the cavity is resonant with a transition. This effect is named after its discoverer, Edward Purcell. If the atom lies in an antinode of the cavity mode, the ratio between the rate of spontaneous emission in the cavity $\Gamma_{sp,cav}$ and Γ_{cav} is

  $$\frac{\Gamma_{sp,cav}}{\Gamma_{cav}} = \frac{3}{4\pi^2}\frac{Q\lambda^3}{V_{mode}}. \tag{B.4}$$

  This ratio is called Purcell factor and shows how to improve enhancement of spontaneous emission: one needs to maximize the Q-factor and minimize mode volume.